



Since January 2020 Elsevier has created a COVID-19 resource centre with free information in English and Mandarin on the novel coronavirus COVID-19. The COVID-19 resource centre is hosted on Elsevier Connect, the company's public news and information website.

Elsevier hereby grants permission to make all its COVID-19-related research that is available on the COVID-19 resource centre - including this research content - immediately available in PubMed Central and other publicly funded repositories, such as the WHO COVID database with rights for unrestricted research re-use and analyses in any form or by any means with acknowledgement of the original source. These permissions are granted for free by Elsevier for as long as the COVID-19 resource centre remains active.



Research paper

Drug repurposing: Discovery of troxipide analogs as potent antitumor agents

Nan Lu^{b,1}, Jin-ling Huo^{a,1}, Shuai Wang^{a,c,1}, Xiao-Han Yuan^a, Hong-Min Liu^{a,*}^a School of Pharmaceutical Sciences, Zhengzhou University, Zhengzhou, 450001, China^b Department of Pharmacy, University of Copenhagen, Universitetsparken 2, 2100, Copenhagen, Denmark^c Gordon Center for Medical Imaging, Massachusetts General Hospital and Harvard Medical School, Boston, MA, 02129, USA

ARTICLE INFO

Article history:

Received 29 April 2020

Received in revised form

14 May 2020

Accepted 14 May 2020

Available online 26 June 2020

Keywords:

1, 2, 4] triazolo[1, 5-*a*] pyrimidines

Apoptosis

Antiproliferative activity

Drug repurposing

ABSTRACT

Drug repurposing plays a vital role in the discovery of undescribed bioactivities in clinical drugs. Based on drug repurposing strategy, we for the first time reported a novel series of troxipide analogs and then evaluated their antiproliferative activity against MCF-7, PC3, MGC-803, and PC9 cancer cell lines and WPMY-1, most of which showed obvious selectivity toward PC-3 over the other three cancer cell lines and WPMY-1. Compound **5q**, especially, could effectively inhibit PC3 with an IC₅₀ value of 0.91 μM, which exhibited around 53-fold selectivity toward WPMY-1. Data indicated that **5q** effectively inhibited the colony formation, suppressed the cell migration, and induced G1/S phase arrest in PC3 cells. Also, compound **5q** induced cell apoptosis by activating the two apoptotic signaling pathways in PC3 cells: death receptor-mediated extrinsic pathway and mitochondria-mediated intrinsic pathway. Compound **5q** up-regulated the expression of both pro-apoptotic Bax and P53, while down-regulated anti-apoptotic Bcl-2 expression. Besides, compound **5q** significantly increased the expression of cleaved caspase 3/9 and cleaved PARP. Therefore, the successful discovery of compound **5q** may further validate the feasibility of this theory, which will encourage researchers to reveal undescribed bioactivities in traditional drugs.

© 2020 Elsevier Masson SAS. All rights reserved.

1. Introduction

The rapid development of technology and enhanced knowledge of human diseases fails to meet therapeutic advances, since the new drug discovery will be subjected to the high attrition, plenty of costs, and slow pace process [1,2]. Drug repurposing, an effective strategy for the discovery of undescribed bioactivities in clinical drugs, has attracted a lot of researchers to devote themselves to seeking novel applications of traditional drugs, which offers many advantages over the development of an entirely novel drug [1,3]. First, the most important advantage of drug repurposing is the lower risk of failure due to the fact that the repurposed drug has been validated safe enough in preclinical models and humans. Second, as most of the preclinical testing and safety assessment has already been completed, the required length of time for novel drug development will be significantly reduced. Third, the costs of the overall development of the repurposing candidate will markedly decrease due to the above

two advantages. The proportion of drugs developed based on drug repurposing theory is probably around 75% [4]. Historically, drug repurposing strategy has achieved great success, resulting in a lot of promising candidate drugs, some of which have been used for the treatment of both common and rare diseases [5–8]. As one of the most successful examples of drug repurposing so far, sildenafil citrate, originally developed as an antihypertensive drug by Pfizer, was repurposed for the effective treatment of erectile dysfunction [9]. Thalidomide, originally used for the treatment of sedative in 1957, was infamous for its serious side effect of leading to severe skeletal birth defects in children born to mothers who had taken the drug the first trimester of their pregnancies, which was serendipitously discovered to be effective for the treatment of multiple myeloma [10], subsequently generating some more successful derivatives, such as lenalidomide, with worldwide sales of up to \$8.2 billion in 2017 [11]. Based on drug repurposing strategy, dolutegravir and dictegravir, anti-HIV drugs targeting integrase, were developed as the first PA endonuclease inhibitor—Baloxavir marboxil, which was approved in 2018 by Japan for the treatment of influenza A and B virus infections in paediatric and adult patients [12]. Besides, given the pretty severe situation facing the world, there is still no approved effective drug against

* Corresponding author.

E-mail address: liuhm@zzu.edu.cn (H.-M. Liu).¹ Nan Lu, Jin-ling Huo, and Shuai Wang contributed equally to this work.

COVID-19. How to quickly obtain effective compounds for the treatment of COVID-19 remains a challenge. Therefore, drug repurposing, as a fast and effective strategy to reveal new indications of traditional drugs, has been successfully exploited to identify novel application of 'old' drugs for the treatment of COVID-19, generating some potent candidates, such as chloroquine or hydroxychloroquine, Remdesivir, Favipiravir, and Tocilizumab [13,14]. Chloroquine or hydroxychloroquine, clinically used as an antimalarial drug, has been found to effectively inhibit COVID-19 *in vitro* [15,16]. As an antiviral agent, Remdesivir, initially researched in Ebola virus clinical studies, showed potent inhibitory activity against COVID-19 *in vitro* [17]. Besides, Favipiravir, previously approved by Japan for the treatment of anti-flu drug, was validated to be safe and effective for the treatment of COVID-19 patients [14]. Tocilizumab, clinically used as an immunosuppressive agent in the clinic, was discovered to be effective for the treatment of COVID-19 patients *in vivo* [18]. All these discovered drugs need to be subjected to further testing to avoid unexpected side effects.

Troxipide, clinically used in the treatment of gastroesophageal reflux disease, has been reported to have anti-inflammatory properties, which has not been found any reports related to tumor so far [19]. In addition, our previous work has indicated that [1,2,4]triazolo [1,5-a]pyrimidine fragment possesses various pharmaceutical properties [20–24], making it promising in drug design. In this work, we performed drug repurposing strategy to design and synthesize a novel series of troxipide derivatives by introducing [1,2,4]triazolo [1,5-a]pyrimidine with different substituents to troxipide, hopefully achieving some promising compounds with interesting bioactivities, leading to the identification of the most potent compound **5q** (Fig. 1).

2. Results and discussion

2.1. Chemistry

The synthetic routes for the synthesis of compounds 5a-5v. Compounds **4a-4v** were obtained by following the previously reported method [23]. As depicted in Scheme 1, compounds **2a-2s** were obtained by reacting 5-amino-4H-1,2,4-triazole-3-thiol with different alkyl halides, followed by refluxing with various β -ketoesters in acetic acid, respectively, giving compounds **3v-3v**, which were further subjected to chlorination by POCl₃, affording compounds **4a-4v**. Finally, compounds **4a-4v** reacted with commercially available Troxipide to give compounds **5a-5v**.

2.2. Biochemical evaluation of troxipide analogs

Initially, the first troxipide analog **5a** was obtained by introducing [1,2,4]triazolo [1,5-a]pyrimidines group to troxipide based on drug repurposing strategy. We next screened its antitumor activities against four different kinds of cancer cell lines, namely, MCF-7 (human breast cancer cell line), PC3 (human prostatic carcinoma cell line), MGC-803 (human gastric cancer cell line), and PC9 (human lung cancer cell line) by the MTT assay, taking 5-Fu and troxipide as the controls. Intriguingly, compound **5a** displayed acceptable antiproliferative activity toward the four selected cell lines, but less potent than that of 5-Fu, while troxipide showed no any activity (IC₅₀ > 100 μ M) (Table 1). Encouraged by the interesting result, we next performed further structural modification around the different positions of the [1,2,4]triazolo [1,5-a]pyrimidines group, giving compounds **5a-5v**. All these compounds were evaluated for their antitumor efficacy against MCF-7, PC3, MGC-803, and PC9 cancer cell lines, respectively, and 5-Fu was chosen as a positive control. As shown in Table 1, compounds **5a-5v** displayed weak to strong inhibitory activity against the selected cancer cells, and it was worth noting that all of these compounds showed obvious selectivity toward PC3 over the other three cancer cell lines, except compound **5s**. Therefore, in the following structural modifications, we mainly concentrated on the effect of compounds **5a-5v** on PC3.

Firstly, we focused primarily on the molecular fine-tuning of substituents on the phenyl of compound **5a**, generating compounds **5b-5n**, most of which displayed moderate to strong inhibitory activity against PC3. Compared to compound **5a** and 5-Fu, compounds **5b-5d**, **5g**, and **5k**, bearing electron-withdrawing group at the 4-position of phenyl in compound **5a**, showed pretty strong inhibitory activity against PC3 while compound **5h**, with pretty strong electron-withdrawing -CF₃ group at the 4-position of phenyl, exhibited reduced activity. Whether moving 4-Br to 2-Br or 3-Br of the phenyl in compound **5d**, resulting in compound **5e** and **5f**, led to the decrease of inhibitory activity toward PC3. Similarly, both compounds **5i** (2-CF₃) and **5j** (4-CF₃) significantly decreased the inhibitory activity toward PC3 compared with compound **5h** (4-CF₃). Besides, incorporation of a methoxy group at the 4-position of the phenyl in compound **5a** giving compound **5l** induced a sharp decrease of activity, while compound **5m**, bearing methyl group at the 4-position of the phenyl, exhibited almost comparable activity toward PC3 with compound **5a**. Besides, compound **5n**, with 2,6-diCl groups at the phenyl in compound **5a**,

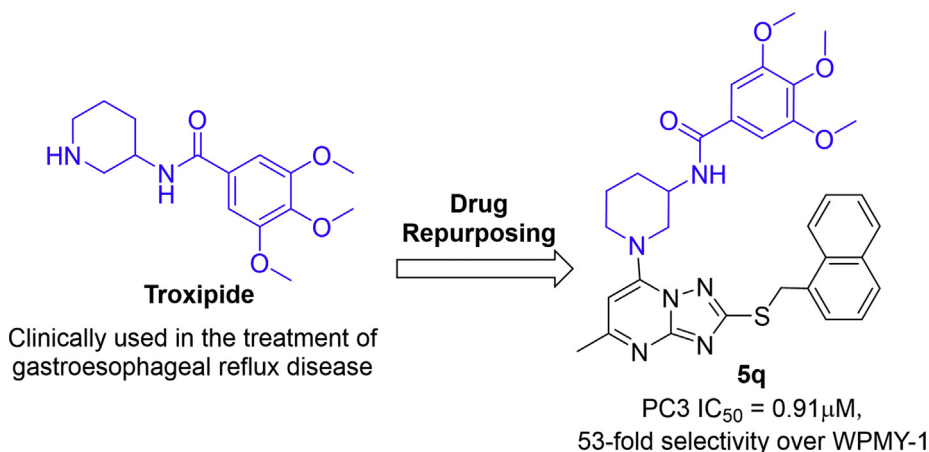
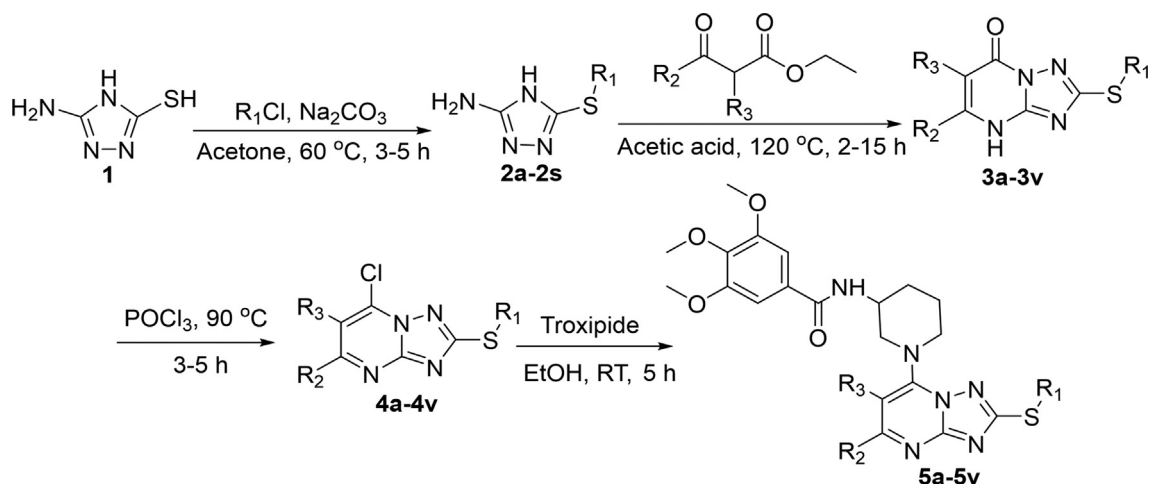


Fig. 1. Design of Troxipide analog **5q** based on the Drug Repurposing strategy.



Scheme 1. Synthesis of compounds 5a-5v.

also displayed moderate antitumor activity toward PC3, which was less potent than compound **5c**. Taken together, these data suggested that the introduction of moderate electron-withdrawing group at the 4-position of the phenyl in compound **5a** was favorable for increasing the antiproliferative activity toward PC3. To further investigate the SARs, we investigated the effect of the number of methylene between sulfhydryl and Phenyl on the inhibitory activity, giving compounds **5o-5p**. Unfortunately, both of them showed significantly decreased inhibitory activity toward PC3, suggesting the number of methylene between sulfhydryl and Phenyl was necessary for the activity. Intriguingly, replacement of the phenyl with bulky group naphthalene in compound **5a** resulted in compound **5o**, which could significantly inhibit PC3 with an IC_{50} value of 0.91 μ M, about 5.8-fold more potent than 5-Fu. However, replacement of the phenyl group with small alkyl group n-propylene in compound **5a** gave compound **5r**, which led to significant loss of antiproliferative activity. Besides, replacement of the phenyl group with heterocyclic group benzimidazole in compound **5a**, generating compound **5s**, exhibited improved anticancer efficacy toward PC3 but less than that of compound **5q**, while compound **5s** showed much better inhibitory activity toward MCF-7, MGC-803, and PC9 than compound **5a**.

Also, we next explored the effect of the size of R_2 on the antiproliferative activity toward PC3 by replacing the methyl group at R_2 in compound **5c** with ethyl or Phenyl group, respectively, producing compounds **5t-5u**. Compound **5t** showed almost the same inhibitory activity as compound **5c** toward PC3 while compound **5u** displayed significantly decreased antiproliferative activity, indicating the bulky group such as phenyl group at R_2 was not favorable for other for the antitumor activity. To the end, one n-pentane group was also incorporated into the position of R_3 in compound **5c** to further investigate the SARs, generating compound **5v**, which led to a sharp decrease of the antiproliferative activity toward PC3.

Given the encouraging results, troxipide analogs **5a-5v** have further tested their possible toxicity toward the WPMY-1 (normal human prostatic stromal myofibroblast cell line), taking **5-Fu** as the control. As depicted in Table 2, compounds **5a-5v** displayed moderate to weak toxicity toward WPMY-1. Compound **5q**, especially, showed pretty weak inhibitory activity toward WPMY-1 with an IC_{50} value of 48.15 μ M while it could effectively inhibit PC3 (IC_{50} = 0.91 μ M), showing up to 53-fold selectivity, which exhibited obvious advantages over **5-Fu** (see Table 2).

2.3. The effect of compound 5q on colony formation and cell cycle distribution of PC3

Encouraged by the potent antiproliferative activity of compound **5q** against PC3, we next evaluated the inhibitory activity of compound **5q** against PC3 at 24 h, 48 h, and 72 h, respectively. The results demonstrated that compound **5q** significantly inhibited the proliferation of PC3 cells dose- and time-dependently (Fig. 2A). Subsequently, colony formation assay was performed, and we found that cells incubated with 0.125 μ M, 0.25 μ M, and 0.5 μ M compound **5q** formed fewer and smaller colonies (Fig. 2B & C). Inducement of cell cycle arrest is an important method of human anti-tumor therapy [25,26]. Therefore, we tested the effect of different concentrations of compound **5q** on the cell cycle in PC3 cells using flow cytometry. As shown in Fig. 2D & E, compound **5q** significantly increased the G1/S phase population while decreased G2/M content at high concentration in PC3 cells. It has been reported that p27 is a cyclin-dependent kinase inhibitor and its expression level can reflect cell cycle progression [27]. Therefore, we further explored the effect of compound **5q** on the expression of p27 by western blotting. As depicted in Fig. 2F & G, compound **5q** dose-dependently elevated the expression of p27. The data revealed that the antiproliferative activity of compound **5q** toward PC3 cells was associated with the G1/S cell cycle arrest.

2.4. The effect of compound 5q on apoptosis of PC3 cells

To further explore the cytotoxicity of compound **5q** on PC3 cells, we further investigated the mechanism of inhibitory efficacy of compound **5q** on PC3 cells. Firstly, Hoechst 33342 staining was carried out to examine the effect of compound **5q** on cell apoptosis. As shown in Fig. 3A & B, PC3 cells treated with compound **5q** at the indicated concentrations displayed apoptosis-associated morphologies, such as cell rounding up, chromatin condensation, and formation of apoptotic bodies. Next, Annexin V-FITC/PI apoptosis detection kit was utilized to examine the apoptosis of PC3 cells using flow cytometry. As shown in Fig. 3C & D, treatment of PC3 with compound **5q** at different concentrations (1, 2, and 4 μ M) dose-dependently led to significant increase of FITC-Annexin V/PI positive population, and especially the treatment of PC3 by compound **5q** at 4 μ M, the apoptotic percentage was up to 70.7%, which was far higher than the control group (3.5%).

Table 1
In vitro inhibitory activity of compound **5a-5v** against the selected cancer cells.

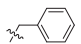
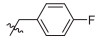
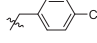
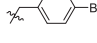
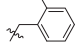
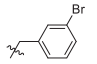

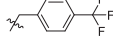
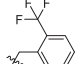
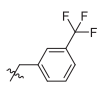
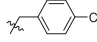
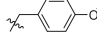
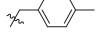
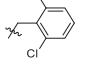
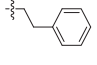
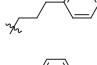
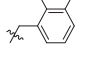
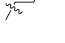
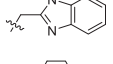
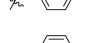
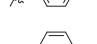

Compound	R ₁	R ₂	R ₃	IC ₅₀ Value (μM)			
				MCF-7	PC3	MGC-803	PC9
5a		-Me	-H	12.21 ± 0.72	7.86 ± 0.69	28.89 ± 0.84	41.41 ± 1.06
5b		-Me	-H	10.45 ± 0.16	4.23 ± 0.35	23.69 ± 0.57	23.38 ± 0.53
5c		-Me	-H	5.20 ± 0.18	1.53 ± 0.42	8.57 ± 0.55	33.00 ± 0.48
5d		-Me	-H	8.56 ± 0.41	1.87 ± 0.27	10.30 ± 0.52	39.27 ± 0.63
5e		-Me	-H	13.35 ± 0.53	8.87 ± 0.46	14.84 ± 0.68	24.24 ± 0.63
5f		-Me	-H	24.87 ± 0.06	11.64 ± 0.21	34.59 ± 0.66	>50
5g		-Me	-H	6.61 ± 0.42	2.22 ± 0.09	13.19 ± 0.50	>50
5h		-Me	-H	16.49 ± 1.22	10.46 ± 1.02	26.38 ± 1.21	>50
5i		-Me	-H	>50	25.09 ± 0.34	>50	>50
5j		-Me	-H	23.59 ± 0.20	26.10 ± 0.52	32.92 ± 0.47	>50
5k		-Me	-H	5.79 ± 0.25	1.89 ± 0.03	14.73 ± 0.67	36.21 ± 0.79
5l		-Me	-H	>50	24.35 ± 0.80	>50	>50
5m		-Me	-H	17.16 ± 0.71	13.38 ± 0.37	30.37 ± 0.52	>50
5n		-Me	-H	12.62 ± 0.42	4.56 ± 0.19	13.13 ± 0.48	45.32 ± 0.73
5o		-Me	-H	36.98 ± 0.60	19.79 ± 0.25	35.59 ± 0.41	>50
5p		-Me	-H	>50	28.75 ± 0.24	32.06 ± 0.49	>50
5q		-Me	-H	11.54 ± 0.18	0.91 ± 0.31	8.21 ± 0.50	34.68 ± 0.67
5r		-Me	-H	>50	>50	>50	>50
5s		-Me	-H	3.55 ± 0.55	6.30 ± 0.11	4.02 ± 0.48	10.37 ± 0.64
5t		-Ethyl	-H	5.74 ± 0.12	2.18 ± 0.07	10.62 ± 0.42	43.48 ± 0.54
5u		-Ph	-H	>50	15.81 ± 0.26	28.50 ± 0.54	>50
5v		-Me	n-pentane	>50	29.65 ± 0.22	>50	>50
5-Fu	—	—	—	4.55 ± 1.03	5.32 ± 1.17	6.52 ± 1.06	4.12 ± 0.83
Troxipide	—	—	—	>100	>100	>100	>100

Table 2
In vitro inhibitory activity of compound **5a-5v** against WPMY-1.

Compound	IC ₅₀ (μM) WPMY-1	Compound	IC ₅₀ (μM) WPMY-1
5a	44.86 ± 0.69	5m	34.29 ± 0.63
5b	30.22 ± 0.34	5n	28.24 ± 0.35
5c	29.55 ± 0.40	5o	37.44 ± 0.38
5d	31.48 ± 0.17	5p	>50
5e	>50	5q	48.15 ± 0.33
5f	41.55 ± 0.19	5r	>50
5g	32.72 ± 0.43	5s	>50
5h	>50	5t	39.56 ± 0.19
5i	42.27 ± 0.35	5u	45.25 ± 0.72
5j	33.47 ± 0.39	5v	>50
5k	>50	5-Fu	8.32 ± 0.97
5l	36.27 ± 0.87		

It has been reported that the accumulation of reactive oxygen species (ROS), the main source of mitochondrial metabolism, could induce cellular apoptosis through a mitochondrial-dependent pathway [28]. So we next explored the effect of compound **5q** on the level of intracellular ROS by using DCFH-DA. As shown in Fig. 3E & F, compound **5q** could effectively increase the accumulation of intracellular ROS in a concentration-dependent manner, which at 4 μM led to 2-fold increase compared with the control. The data indicated that compound **5q** could induce the accumulation of ROS which contributed to the apoptosis of PC3 cells.

Apoptosis has been reported to be mainly mediated by the mitochondria-mediated intrinsic pathway and the death receptor-mediated extrinsic pathway [29]. To further investigate the underlying molecular mechanisms of compound **5q** on the apoptosis of PC3 cells, we next tested the apoptosis-related proteins affected by compound **5q** based on western blotting assay. As shown in Fig. 4A–D, compound **5q** markedly elevated the expression of pro-apoptotic Bax and P53 while anti-apoptotic Bcl-2 expression was down-regulated.

Besides, upon apoptotic stimulation, caspase-9, a member of the cysteine aspartic acid protease (caspase) family, performs interaction with cytochrome C and then it mediates activation of caspase-9. Cleaved caspase-9 further processes other caspase members, such as caspase-3, which is responsible for the proteolytic cleavage of the nuclear enzyme poly (ADP-ribose) polymerase (PARP). They all interact to initiate a caspase cascade and eventually leads to cell apoptosis [30]. As shown in Fig. 4A–D, compound **5q** significantly increased the expression of cleaved caspase 3/9 and cleaved PARP in a dose-dependent manner. These findings demonstrated that compound **5q** could induce the apoptosis of PC3 cells through activating the two apoptotic signaling pathways simultaneously.

2.5. The effect of compound **5q** on the migration of PC3 cells

Cancer metastasis represents an advanced stage of malignancy and is the leading cause of cancer-related deaths while cell migration is involved in cancer metastasis [31,32]. Inhibition of tumor cell migration is an important strategy for the treatment of various cancers in the clinic. Therefore, we evaluated whether compound **5q** affected the inhibition of the migration of PC3 cells. As shown in Fig. 5A–D, the wound healing assay indicated that compound **5q** effectively inhibited the wound healing in a dose-dependent manner, while transwell assay demonstrated that compound **5q** could also significantly inhibit the migration of PC3 cells concentration-dependently.

3. Conclusions

In this work, we for the first time reported a novel series of troxipide analogs and then evaluated their antiproliferative activity against MCF-7, PC3, MGC-803, and PC9 cancer cell lines and WPMY-1, most of which showed obvious selectivity toward PC-3 over the other three cancer cell lines and WPMY-1. Among these analogs, compound **5q** could effectively inhibit PC3 with an IC₅₀ value of 0.91 μM, which exhibited around 53-fold selectivity toward WPMY-1. Biological studies indicated that **5q** could effectively inhibit the colony formation, suppress the cell migration, and induce G1/S phase arrest in PC3 cells. What's more, compound **5q** could induce cell apoptosis by activating the two apoptotic signaling pathways in PC3 cells: death receptor-mediated extrinsic pathway and mitochondria-mediated intrinsic pathway. Compound **5q** could up-regulate the expression of both pro-apoptotic Bax and P53, but down-regulate anti-apoptotic Bcl-2 expression. Besides, compound **5q** could significantly increase the expression of cleaved caspase 3/9 and cleaved PARP. Therefore, the successful application of drug repurposing strategy may further encourage researchers to reveal undescribed indications in clinical drugs.

4. Experimental section

4.1. General information

Reagents and solvents were purchased from commercial sources and used without further purification. Thin-layer chromatography (TLC) was carried out on glass plates coated with silica gel (Qingdao Haiyang Chemical Co., G60F-254) and visualized by UV light (254 nm). The products were purified by column chromatography over silica gel (Qingdao Haiyang Chemical Co., 200–300 mesh). Melting points were determined on an X-5 micromelting apparatus and are uncorrected. All the NMR spectra were recorded with a Bruker DPX 400 MHz spectrometer with TMS as the internal standard in CDCl₃ or DMSO-*d*₆. Chemical shifts are given as δ ppm values relative to TMS. High-resolution mass spectra (HRMS) were recorded on a Waters Micromass Q-T of Micromass spectrometer by electrospray ionization (ESI).

4.2. The general method for the synthesis of **1a-1k**, **2a-2q**, and **3a-3q**

Compounds **2a-2s**, **3a-3v**, and **4a-4v** were prepared following the previously reported method [21].

4.3. The general method for the synthesis of **5a-5v**

N-(1-(2-(benzylthio)-5-methyl-[1,2,4]triazolo [1,5-a]pyrimidin-7-yl)piperidin-3-yl)-3,4,5-trimethoxybenzamide (**5a**), white solid, yield: 84%. m.p.: 146–148 °C. ¹H NMR (400 MHz, DMSO-*d*₆) δ 8.37 (d, *J* = 7.3 Hz, 1H), 7.42 (d, *J* = 7.4 Hz, 2H), 7.34–7.20 (m, 3H), 7.17 (s, 2H), 5.49 (s, 1H), 4.38 (s, 2H), 4.11 (s, 1H), 3.81 (s, 6H), 3.70 (s, 3H), 3.33 (d, *J* = 11.6 Hz, 1H), 3.21 (d, *J* = 12.5 Hz, 1H), 2.79 (dd, *J* = 13.9, 7.2 Hz, 2H), 2.17 (s, 3H), 1.96–1.82 (m, 2H), 1.62 (m, 2H). ¹³C NMR (100 MHz, DMSO-*d*₆) δ 165.93, 160.98, 160.36, 158.41, 157.47, 153.02, 140.67, 138.82, 129.78, 129.27, 128.82, 127.49, 105.52, 96.04, 60.58, 56.53, 47.62, 44.79, 44.00, 34.90, 28.95, 23.90, 22.09. HRMS (ESI): *m/z* calcd for C₂₈H₃₂N₆NaO₄S (M + Na)⁺, 571.2103; found, 571.2102.

N-(1-(2-((4-fluorobenzyl)thio)-5-methyl-[1,2,4]triazolo [1,5-a]pyrimidin-7-yl)piperidin-3-yl)-3,4,5-trimethoxybenzamide (**5b**), white solid, yield: 87%. m.p.: 150–152 °C. ¹H NMR (400 MHz, DMSO-*d*₆) δ 8.37 (d, *J* = 7.4 Hz, 1H), 7.51–7.42 (m, 2H), 7.17 (s, 2H), 7.11 (t, *J* = 8.6 Hz, 2H), 5.49 (s, 1H), 4.38 (s, 2H), 4.13 (d, *J* = 6.5 Hz,

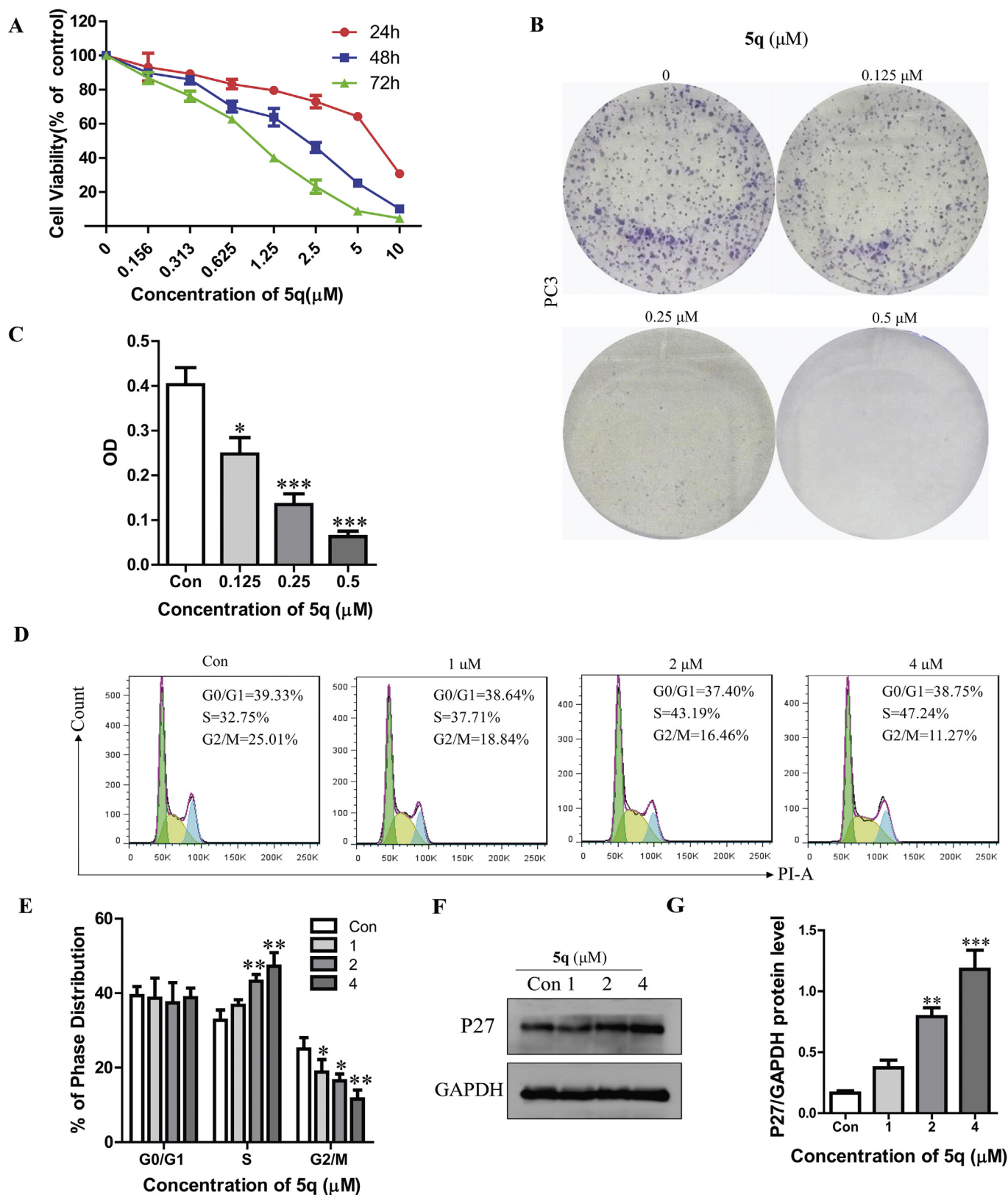


Fig. 2. The effect of Compound 5q on colony formation and cell cycle distribution of PC3 (A) The cell viabilities of PC3 cells treated with different concentrations of compound 5q for 24 h, 48 h, and 72 h, respectively by MTT assay. (B, C) The colony formation and absorbance analysis of crystal violet in PC3 cells treated with indicated concentrations of compound 5q for 6 days. (D, E) PC3 cells were treated with compound 5q at the indicated concentrations for 24 h and the cell cycle distributions were then analyzed by flow cytometry. (F, G) The expression and quantitative analysis of p27 protein in PC3 cells treated with compound 5q at the indicated concentrations for 24 h by western blotting. Three independent experiments were performed. All data were expressed as the mean \pm SEM. * $p < 0.05$, ** $p < 0.01$, *** $p < 0.001$ compared to the control group. (For interpretation of the references to colour in this figure legend, the reader is referred to the Web version of this article.)

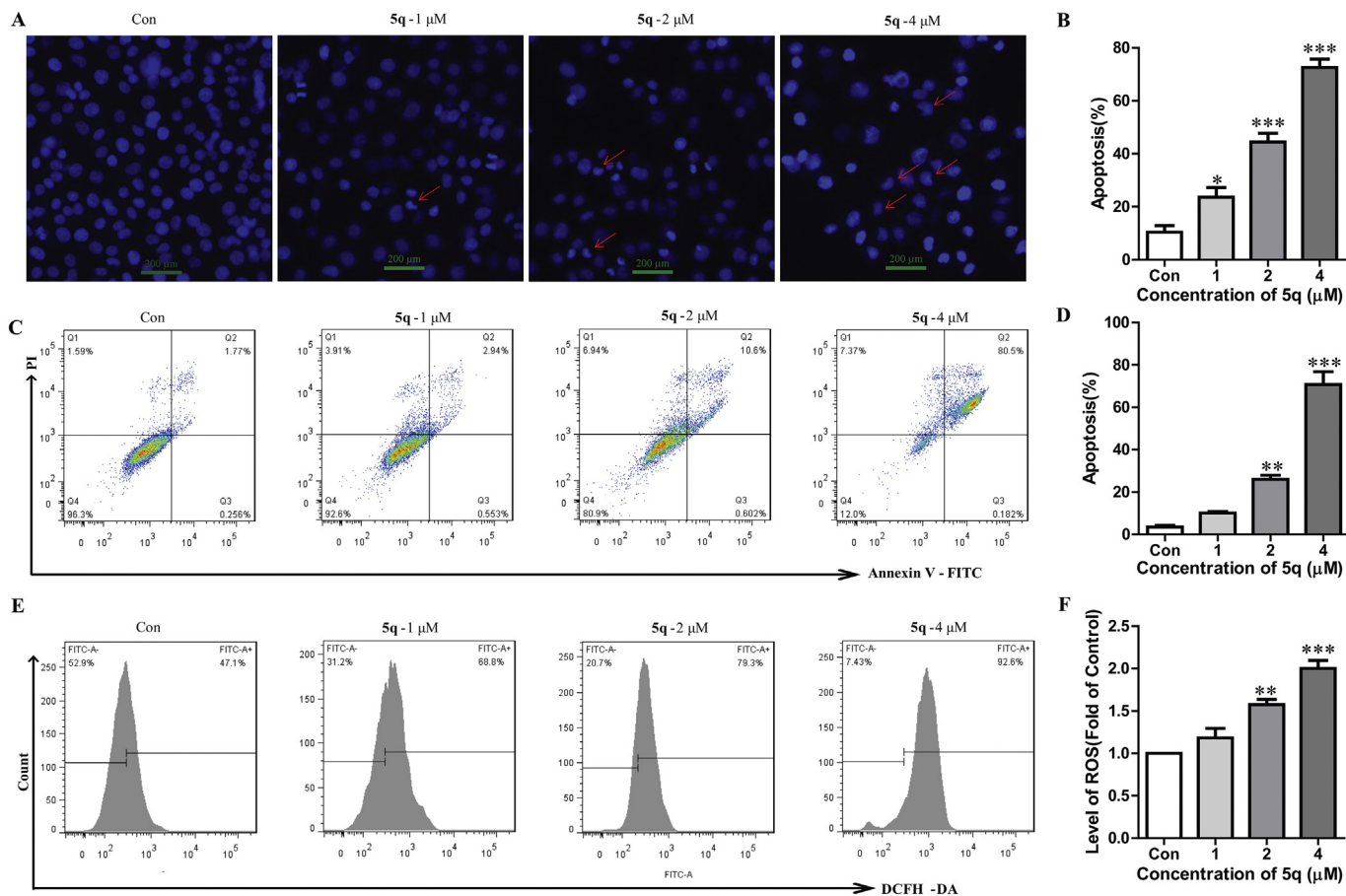


Fig. 3. The effect of compound 5q on apoptosis of PC3 cells and cellular ROS. (A, B) The apoptotic morphological changes (marked with red arrows) and the quantitative analysis of PC3 cells treated with different concentrations of compound 5q for 48h, respectively, by Hoechst 33342 staining. (C, D) The quantitative analysis of PC3 cells treated with compound 5q at the indicated concentrations for 48h, respectively, using Annexin V-FITC/PI double staining through flow cytometry. (E, F) The quantitative analysis of the levels of ROS in PC3 cells treated with different concentrations of compound 5q for 24 h, respectively, by flow cytometry. Three independent experiments were performed. All data were expressed as the mean ± SEM. *p < 0.05, **p < 0.01, ***p < 0.001 compared to the control group. (For interpretation of the references to colour in this figure legend, the reader is referred to the Web version of this article.)

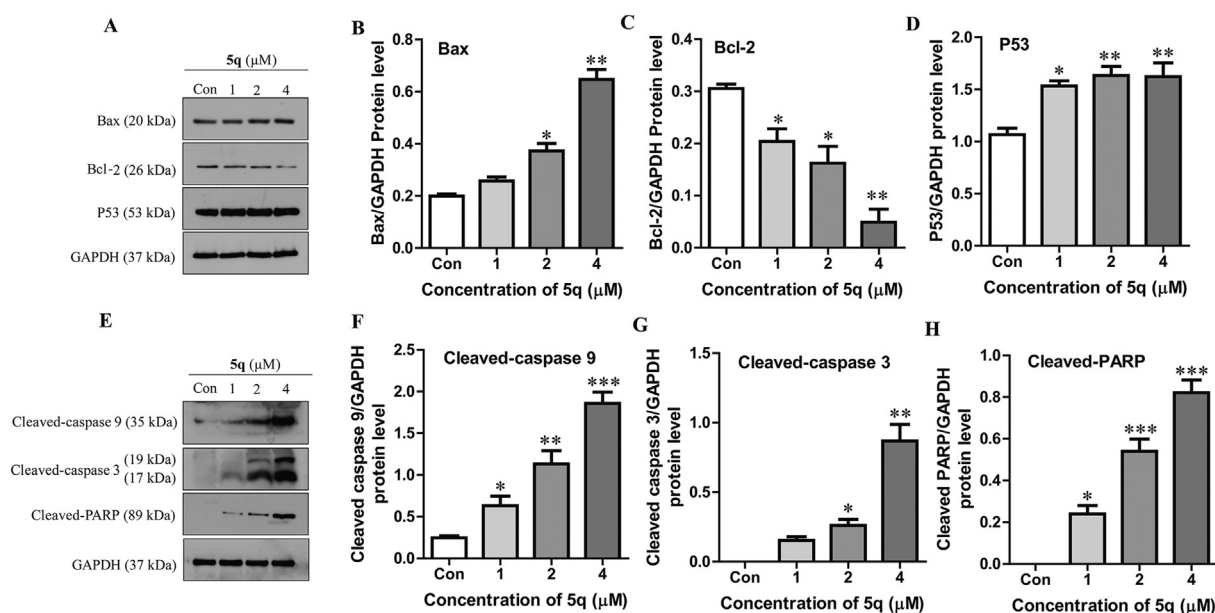


Fig. 4. The effect of compound 5q on apoptosis-related proteins. (A, B, C, D) Expression and quantitative analysis of Bax, Bcl-2, and P53 in PC3 cells treated with compound 5q at the indicated concentrations for 48h. (E, F, G, H) Expression and quantitative analysis of Cleaved-caspase 9/3 and cleaved-PARP in PC3 cells treated with compound 5q at the indicated concentrations for 48h. Three independent experiments were performed. All data were expressed as the mean ± SEM. *p < 0.05, **p < 0.01, ***p < 0.001 compared to the control group.

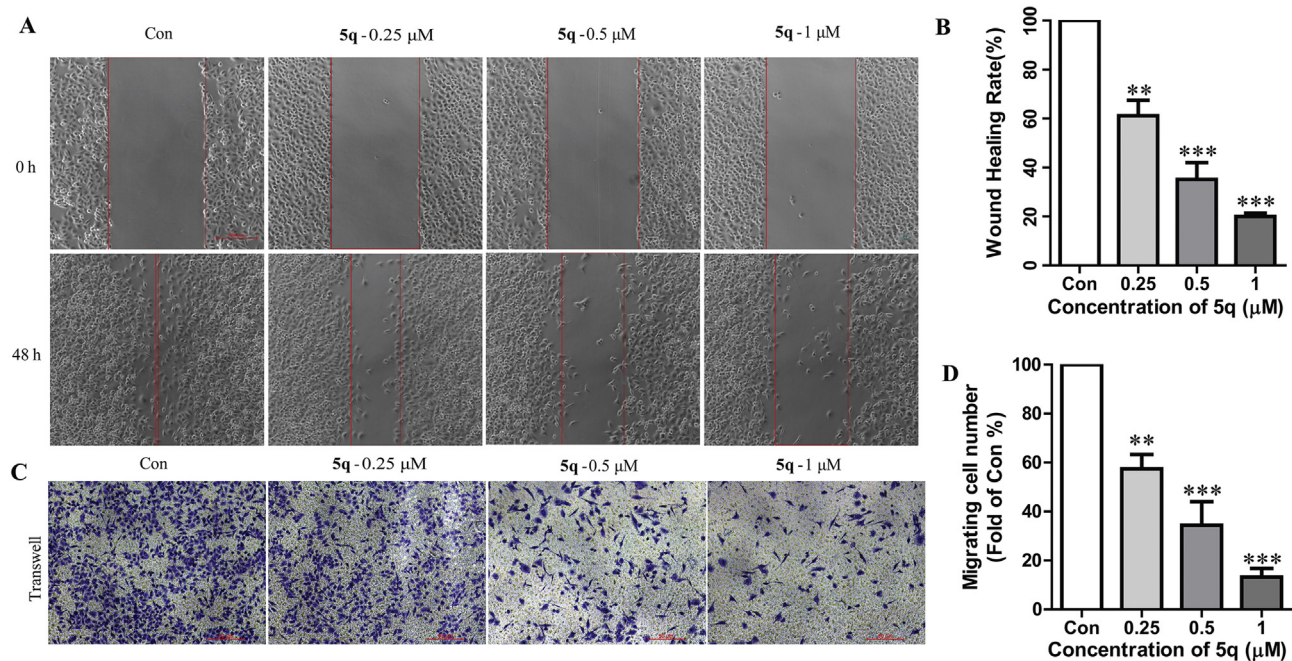


Fig. 5. The effect of compound 5q on the migration ability of PC3 cells. (A, B) Effect and statistical analysis of migration in PC3 cells treated with compound 5q at the indicated concentrations for 48h in wound healing assay. (C, D) Effect and statistical analysis of migration in PC3 cells treated with different concentrations of compound 5q for 48h in transwell assay. Three independent experiments were performed. All data were expressed as the mean \pm SD. ** p < 0.01, *** p < 0.001 compared to Con group.

1H), 3.82 (s, 6H), 3.70 (s, 3H), 3.34 (d, J = 11.7 Hz, 1H), 3.22 (d, J = 12.5 Hz, 1H), 2.80 (dd, J = 20.5, 9.8 Hz, 2H), 2.17 (s, 3H), 1.96–1.84 (m, 2H), 1.72–1.56 (m, 2H). ^{13}C NMR (100 MHz, DMSO- d_6) δ 165.94, 162.92, 160.83, 160.22, 158.31, 157.42, 153.02, 140.69, 135.26, 135.23, 131.24, 131.15, 129.76, 115.64, 115.43, 105.53, 96.09, 60.57, 56.54, 47.54, 44.73, 43.95, 34.00, 28.90, 23.82, 22.01. HRMS (ESI): m/z calcd for $\text{C}_{28}\text{H}_{31}\text{FN}_6\text{NaO}_4\text{S}$ (M + Na) $^+$, 589.2009; found, 589.2009.

N-(1-(2-((4-chlorobenzyl)thio)-5-methyl-[1,2,4]triazolo [1,5-a]pyrimidin-7-yl)piperidin-3-yl)-3,4,5-trimethoxybenzamide (**5c**), white solid, yield: 93%. m.p.: 143–145 °C. ^1H NMR (400 MHz, DMSO- d_6) δ 8.36 (d, J = 7.4 Hz, 1H), 7.45 (d, J = 7.9 Hz, 2H), 7.34 (d, J = 8.0 Hz, 2H), 7.17 (s, 2H), 5.48 (s, 1H), 4.37 (s, 2H), 4.11 (s, 1H), 3.82 (s, 6H), 3.70 (s, 3H), 3.33 (d, J = 11.4 Hz, 1H), 3.20 (d, J = 12.5 Hz, 1H), 2.79 (dd, J = 20.7, 9.9 Hz, 2H), 2.17 (s, 3H), 1.95–1.82 (m, 2H), 1.70–1.53 (m, 2H). ^{13}C NMR (100 MHz, DMSO- d_6) δ 165.92, 160.65, 160.48, 158.51, 157.46, 153.02, 140.67, 138.26, 132.05, 131.09, 129.77, 128.73, 105.52, 96.03, 60.57, 56.53, 47.65, 44.81, 44.01, 34.02, 28.97, 23.95, 22.13. HRMS (ESI): m/z calcd for $\text{C}_{28}\text{H}_{32}\text{ClN}_6\text{O}_4\text{S}$ (M + H) $^+$, 583.1894; found, 583.1894.

N-(1-(2-((4-bromobenzyl)thio)-5-methyl-[1,2,4]triazolo [1,5-a]pyrimidin-7-yl)piperidin-3-yl)-3,4,5-trimethoxybenzamide (**5d**), white solid, yield: 89%. m.p.: 154–157 °C. ^1H NMR (400 MHz, DMSO- d_6) δ 8.36 (d, J = 7.3 Hz, 1H), 7.47 (d, J = 7.8 Hz, 2H), 7.38 (d, J = 7.9 Hz, 2H), 7.17 (s, 2H), 5.48 (s, 1H), 4.36 (s, 2H), 4.12 (s, 1H), 3.82 (s, 6H), 3.70 (s, 3H), 3.34 (d, J = 11.6 Hz, 1H), 3.21 (d, J = 12.5 Hz, 1H), 2.80 (dd, J = 20.9, 10.1 Hz, 2H), 2.17 (s, 3H), 1.97–1.83 (m, 2H), 1.71–1.56 (m, 2H). ^{13}C NMR (100 MHz, DMSO- d_6) δ 165.93, 160.67, 160.18, 158.30, 157.39, 153.03, 140.69, 138.67, 131.66, 131.45, 129.75, 120.56, 105.53, 96.12, 60.58, 56.55, 47.53, 44.73, 43.95, 34.08, 28.90, 23.80, 22.01. HRMS (ESI): m/z calcd for $\text{C}_{28}\text{H}_{32}\text{BrN}_6\text{O}_4\text{S}$ (M + H) $^+$, 627.1389; found, 627.1390.

N-(1-(2-((2-bromobenzyl)thio)-5-methyl-[1,2,4]triazolo [1,5-a]pyrimidin-7-yl)piperidin-3-yl)-3,4,5-trimethoxybenzamide (**5e**), white solid, yield: 87%. m.p.: 145–148 °C. ^1H NMR (400 MHz, DMSO- d_6) δ 8.36 (d, J = 7.4 Hz, 1H), 7.62 (t, J = 9.0 Hz, 2H), 7.31 (t, J = 7.5 Hz, 1H), 7.25–7.12 (m, 3H), 5.48 (s, 1H), 4.47 (s, 2H), 4.11 (s,

1H), 3.82 (s, 6H), 3.70 (s, 3H), 3.37–3.30 (m, 1H), 3.21 (d, J = 12.6 Hz, 1H), 2.79 (dd, J = 21.6, 10.6 Hz, 2H), 2.17 (s, 3H), 1.90 (t, J = 17.0 Hz, 2H), 1.70–1.55 (m, 2H). ^{13}C NMR (100 MHz, DMSO- d_6) δ 165.92, 160.46, 160.40, 158.47, 157.43, 153.02, 140.67, 137.81, 133.10, 131.64, 129.80, 129.76, 128.31, 124.42, 105.52, 96.08, 60.58, 56.54, 47.60, 44.78, 43.99, 35.54, 28.94, 23.92, 22.08. HRMS (ESI): m/z calcd for $\text{C}_{28}\text{H}_{32}\text{BrN}_6\text{O}_4\text{S}$ (M + H) $^+$, 627.1389; found, 627.1389.

N-(1-(2-((3-bromobenzyl)thio)-5-methyl-[1,2,4]triazolo [1,5-a]pyrimidin-7-yl)piperidin-3-yl)-3,4,5-trimethoxybenzamide (**5f**), white solid, yield: 90%. m.p.: 155–159 °C. ^1H NMR (400 MHz, DMSO- d_6) δ 8.37 (d, J = 7.3 Hz, 1H), 7.65 (s, 1H), 7.48–7.38 (m, 2H), 7.25 (t, J = 7.8 Hz, 1H), 7.17 (s, 2H), 5.49 (s, 1H), 4.38 (s, 2H), 4.12 (s, 1H), 3.82 (s, 6H), 3.70 (s, 3H), 3.34 (d, J = 11.8 Hz, 1H), 3.22 (d, J = 12.5 Hz, 1H), 2.80 (dd, J = 21.7, 10.7 Hz, 2H), 2.17 (s, 3H), 1.95–1.85 (m, 2H), 1.78–1.50 (m, 2H). ^{13}C NMR (100 MHz, DMSO- d_6) δ 165.94, 160.61, 160.20, 158.32, 157.38, 153.02, 142.06, 140.68, 131.88, 130.94, 130.32, 129.75, 128.35, 121.92, 105.53, 96.15, 60.58, 56.54, 47.51, 44.72, 43.94, 34.05, 28.89, 23.81, 22.00. HRMS (ESI): m/z calcd for $\text{C}_{28}\text{H}_{32}\text{BrN}_6\text{O}_4\text{S}$ (M + H) $^+$, 627.1389; found, 627.1387.

3,4,5-trimethoxy-N-(1-(5-methyl-2-((4-nitrobenzyl)thio)-[1,2,4]triazolo [1,5-a]pyrimidin-7-yl)piperidin-3-yl)benzamide (**5g**), white solid, yield: 86%. m.p.: 164–166 °C. ^1H NMR (400 MHz, DMSO- d_6) δ 8.37 (d, J = 7.3 Hz, 1H), 7.45 (d, J = 7.9 Hz, 2H), 7.34 (d, J = 8.0 Hz, 2H), 7.17 (s, 2H), 5.49 (s, 1H), 4.38 (s, 2H), 4.12 (s, 1H), 3.82 (s, 6H), 3.70 (s, 3H), 3.34 (d, J = 11.6 Hz, 1H), 3.22 (d, J = 12.5 Hz, 1H), 2.80 (dd, J = 20.8, 10.0 Hz, 2H), 2.17 (s, 3H), 1.95–1.85 (m, 2H), 1.74–1.54 (m, 2H). ^{13}C NMR (100 MHz, DMSO- d_6) δ 165.93, 160.70, 160.17, 158.28, 157.39, 153.02, 140.69, 138.22, 132.06, 131.09, 129.75, 128.73, 105.53, 96.13, 60.58, 56.54, 47.50, 44.71, 43.93, 34.03, 28.88, 23.79, 21.98. HRMS (ESI): m/z calcd for $\text{C}_{28}\text{H}_{32}\text{N}_7\text{O}_6\text{S}$ (M + H) $^+$, 594.2135; found, 594.2134.

3,4,5-trimethoxy-N-(1-(5-methyl-2-((4-(trifluoromethyl)benzyl)thio)-[1,2,4]triazolo [1,5-a]pyrimidin-7-yl)piperidin-3-yl)benzamide (**5h**), white solid, yield: 79%. m.p.: 159–162 °C. ^1H NMR (400 MHz, DMSO- d_6) δ 8.38 (d, J = 7.4 Hz, 1H), 7.65 (s, 4H), 7.18 (s, 2H), 5.48 (s, 1H), 4.47 (s, 2H), 4.13 (d, J = 6.4 Hz, 1H), 3.82 (s, 6H),

3.70 (s, 3H), 3.34 (d, $J = 11.7$ Hz, 1H), 3.21 (d, $J = 12.7$ Hz, 1H), 2.80 (dd, $J = 19.7, 9.5$ Hz, 2H), 2.17 (s, 3H), 1.95–1.84 (m, 2H), 1.65 (m, 2H). ^{13}C NMR (100 MHz, DMSO- d_6) δ 165.92, 160.47, 160.42, 158.47, 157.43, 153.02, 144.24, 140.68, 129.99, 125.66, 125.62, 105.53, 96.09, 60.56, 56.53, 47.54, 44.72, 43.94, 34.17, 28.89, 23.91, 21.99. HRMS (ESI): m/z calcd for $\text{C}_{29}\text{H}_{32}\text{F}_3\text{N}_6\text{O}_4\text{S}$ ($\text{M} + \text{H}$) $^+$, 617.2158; found, 617.2159.

3,4,5-trimethoxy-N-(1-(5-methyl-2-((2-(trifluoromethyl)benzyl)thio)-[1,2,4]triazolo [1,5-a]pyrimidin-7-yl)piperidin-3-yl)benzamide (**5i**), white solid, yield: 83%. m.p.: 150–152 °C. ^1H NMR (400 MHz, DMSO- d_6) δ 8.36 (d, $J = 7.3$ Hz, 1H), 7.75 (dd, $J = 18.3, 7.8$ Hz, 2H), 7.62 (t, $J = 7.5$ Hz, 1H), 7.49 (t, $J = 7.5$ Hz, 1H), 7.17 (s, 2H), 5.49 (s, 1H), 4.56 (s, 2H), 4.12 (s, 1H), 3.82 (s, 6H), 3.70 (s, 3H), 3.33 (d, $J = 11.6$ Hz, 1H), 3.21 (d, $J = 12.5$ Hz, 1H), 2.79 (dd, $J = 21.8, 10.8$ Hz, 2H), 2.17 (s, 3H), 1.88 (m, 2H), 1.72–1.56 (m, 2H). ^{13}C NMR (100 MHz, DMSO- d_6) δ 165.92, 164.87, 160.48, 158.52, 157.45, 153.02, 140.67, 137.06, 133.28, 132.20, 129.75, 128.37, 126.47, 126.42, 105.52, 96.13, 60.57, 56.53, 47.53, 44.73, 43.94, 31.56, 28.90, 23.95, 22.02, 21.63. HRMS (ESI): m/z calcd for $\text{C}_{29}\text{H}_{32}\text{F}_3\text{N}_6\text{O}_4\text{S}$ ($\text{M} + \text{H}$) $^+$, 617.2158; found, 617.2158.

3,4,5-trimethoxy-N-(1-(5-methyl-2-((3-(trifluoromethyl)benzyl)thio)-[1,2,4]triazolo [1,5-a]pyrimidin-7-yl)piperidin-3-yl)benzamide (**5j**), white solid, yield: 87%. m.p.: 161–163 °C. ^1H NMR (400 MHz, DMSO- d_6) δ 8.37 (d, $J = 7.4$ Hz, 1H), 7.81 (s, 1H), 7.75 (d, $J = 7.5$ Hz, 1H), 7.59 (d, $J = 7.7$ Hz, 1H), 7.53 (t, $J = 7.6$ Hz, 1H), 7.18 (s, 2H), 5.48 (s, 1H), 4.48 (s, 2H), 4.12 (s, 1H), 3.82 (s, 6H), 3.70 (s, 3H), 3.33 (d, $J = 11.8$ Hz, 1H), 3.21 (d, $J = 12.6$ Hz, 1H), 2.80 (dd, $J = 19.1, 8.5$ Hz, 2H), 2.17 (s, 3H), 1.90 (t, $J = 16.6$ Hz, 2H), 1.70–1.57 (m, 2H). ^{13}C NMR (100 MHz, DMSO- d_6) δ 165.92, 160.50, 160.20, 158.51, 157.44, 153.02, 140.85, 140.67, 133.41, 129.83, 129.76, 125.77, 125.73, 124.18, 124.14, 105.52, 96.06, 60.57, 56.54, 47.55, 44.74, 43.96, 34.12, 28.92, 23.95, 22.03. HRMS (ESI): m/z calcd for $\text{C}_{29}\text{H}_{32}\text{F}_3\text{N}_6\text{O}_4\text{S}$ ($\text{M} + \text{H}$) $^+$, 617.2158; found, 617.2156.

N-(1-(2-((4-cyanobenzyl)thio)-5-methyl-[1,2,4]triazolo [1,5-a]pyrimidin-7-yl)piperidin-3-yl)-3,4,5-trimethoxybenzamide (**5k**), white solid, yield: 92%. m.p.: 147–150 °C. ^1H NMR (400 MHz, DMSO- d_6) δ 8.38 (d, $J = 7.3$ Hz, 1H), 7.75 (d, $J = 7.7$ Hz, 2H), 7.63 (d, $J = 7.8$ Hz, 2H), 7.17 (s, 2H), 5.49 (s, 1H), 4.46 (s, 2H), 4.14 (d, $J = 6.7$ Hz, 1H), 3.82 (s, 6H), 3.70 (s, 3H), 3.35 (d, $J = 11.7$ Hz, 1H), 3.23 (d, $J = 12.5$ Hz, 1H), 2.81 (dd, $J = 21.0, 10.1$ Hz, 2H), 2.17 (s, 3H), 1.91 (t, $J = 15.3$ Hz, 2H), 1.74–1.56 (m, 2H). ^{13}C NMR (100 MHz, DMSO- d_6) δ 165.95, 160.40, 160.23, 158.29, 157.37, 153.02, 145.33, 140.69, 132.70, 130.21, 129.72, 119.27, 110.17, 105.52, 96.19, 60.58, 56.54, 47.38, 44.63, 43.87, 34.32, 28.81, 23.79, 21.87. HRMS (ESI): m/z calcd for $\text{C}_{29}\text{H}_{31}\text{N}_7\text{NaO}_4\text{S}$ ($\text{M} + \text{Na}$) $^+$, 596.2056; found, 596.2057.

3,4,5-trimethoxy-N-(1-(2-((4-methoxybenzyl)thio)-5-methyl-[1,2,4]triazolo [1,5-a]pyrimidin-7-yl)piperidin-3-yl)benzamide (**5l**), white solid, yield: 90%. m.p.: 144–148 °C. ^1H NMR (400 MHz, DMSO- d_6) δ 8.39 (d, $J = 7.3$ Hz, 1H), 7.34 (d, $J = 8.0$ Hz, 2H), 7.17 (s, 2H), 6.85 (d, $J = 8.0$ Hz, 2H), 5.51 (s, 1H), 4.33 (s, 2H), 4.14 (d, $J = 6.1$ Hz, 1H), 3.81 (s, 6H), 3.71 (d, $J = 4.3$ Hz, 6H), 3.36 (d, $J = 11.3$ Hz, 1H), 3.24 (d, $J = 12.5$ Hz, 1H), 2.82 (dd, $J = 20.4, 9.9$ Hz, 2H), 2.18 (s, 3H), 1.91 (t, $J = 15.1$ Hz, 2H), 1.74–1.56 (m, 2H). ^{13}C NMR (100 MHz, DMSO- d_6) δ 165.95, 161.24, 159.47, 158.84, 157.76, 157.28, 153.03, 140.70, 130.46, 129.74, 114.25, 105.54, 96.28, 60.58, 56.54, 55.50, 47.37, 44.62, 43.87, 34.46, 28.81, 23.44, 21.85. HRMS (ESI): m/z calcd for $\text{C}_{29}\text{H}_{35}\text{N}_6\text{O}_5\text{S}$ ($\text{M} + \text{H}$) $^+$, 579.2390; found, 579.2390.

3,4,5-trimethoxy-N-(1-(5-methyl-2-((4-methylbenzyl)thio)-[1,2,4]triazolo [1,5-a]pyrimidin-7-yl)piperidin-3-yl)benzamide (**5m**), white solid, yield: 86%. m.p.: 151–154 °C. ^1H NMR (400 MHz, DMSO- d_6) δ 8.38 (d, $J = 7.4$ Hz, 1H), 7.29 (d, $J = 7.5$ Hz, 2H), 7.17 (s, 2H), 7.09 (d, $J = 7.6$ Hz, 2H), 5.50 (s, 1H), 4.34 (s, 2H), 4.14 (d, $J = 6.5$ Hz, 1H), 3.81 (s, 6H), 3.70 (s, 3H), 3.35 (d, $J = 9.7$ Hz, 1H), 3.22 (d, $J = 12.5$ Hz, 1H), 2.81 (dd, $J = 19.9, 9.6$ Hz, 2H), 2.25 (s, 3H), 2.18 (s, 3H), 1.96–1.84 (m, 2H), 1.72–1.55 (m, 2H). ^{13}C NMR (100 MHz,

DMSO- d_6) δ 165.94, 161.12, 159.88, 158.05, 157.37, 153.02, 140.69, 136.66, 135.59, 129.75, 129.38, 129.18, 105.53, 96.16, 60.58, 56.53, 47.46, 44.69, 43.91, 34.71, 28.87, 23.64, 21.94, 21.14. HRMS (ESI): m/z calcd for $\text{C}_{29}\text{H}_{35}\text{N}_6\text{O}_4\text{S}$ ($\text{M} + \text{H}$) $^+$, 563.2440; found, 563.2438.

N-(1-(2-((2,6-dichlorobenzyl)thio)-5-methyl-[1,2,4]triazolo [1,5-a]pyrimidin-7-yl)piperidin-3-yl)-3,4,5-trimethoxybenzamide (**5n**), white solid, yield: 76%. m.p.: 140–142 °C. ^1H NMR (400 MHz, DMSO- d_6) δ 8.36 (d, $J = 7.3$ Hz, 1H), 7.51 (d, $J = 8.0$ Hz, 2H), 7.37 (t, $J = 8.0$ Hz, 1H), 7.17 (s, 2H), 5.50 (s, 1H), 4.66 (s, 2H), 4.11 (s, 1H), 3.81 (s, 6H), 3.70 (s, 3H), 3.34 (d, $J = 11.6$ Hz, 1H), 3.21 (d, $J = 12.5$ Hz, 1H), 2.79 (dd, $J = 21.2, 10.3$ Hz, 2H), 2.18 (s, 3H), 1.95–1.85 (m, 2H), 1.73–1.55 (m, 2H). ^{13}C NMR (100 MHz, DMSO- d_6) δ 165.91, 160.64, 160.48, 158.59, 157.52, 153.01, 140.67, 135.54, 133.21, 130.65, 129.75, 129.18, 105.51, 96.06, 60.57, 56.53, 47.64, 44.79, 44.01, 31.72, 28.95, 24.01, 22.10. HRMS (ESI): m/z calcd for $\text{C}_{28}\text{H}_{31}\text{Cl}_2\text{N}_6\text{O}_4\text{S}$ ($\text{M} + \text{H}$) $^+$, 617.1505; found, 617.1504.

3,4,5-trimethoxy-N-(1-(5-methyl-2-(phenethylthio)-[1,2,4]triazolo [1,5-a]pyrimidin-7-yl)piperidin-3-yl)benzamide (**5o**), white solid, yield: 85%. m.p.: 149–152 °C. ^1H NMR (400 MHz, DMSO- d_6) δ 8.38 (d, $J = 7.3$ Hz, 1H), 7.29 (m, 4H), 7.24–7.14 (m, 3H), 5.50 (s, 1H), 4.13 (d, $J = 6.3$ Hz, 1H), 3.81 (s, 6H), 3.70 (s, 3H), 3.39–3.29 (m, 3H), 3.22 (d, $J = 12.5$ Hz, 1H), 2.99 (t, $J = 7.4$ Hz, 2H), 2.80 (dd, $J = 20.5, 9.9$ Hz, 2H), 2.18 (s, 3H), 1.97–1.82 (m, 2H), 1.73–1.54 (m, 2H). ^{13}C NMR (101 MHz, DMSO) δ 165.93, 161.15, 159.89, 158.15, 157.40, 153.02, 140.77, 140.67, 129.77, 129.02, 128.77, 126.69, 105.52, 96.10, 60.58, 56.53, 47.57, 44.76, 43.97, 35.94, 32.22, 28.93, 23.67, 22.04. HRMS (ESI): m/z calcd for $\text{C}_{29}\text{H}_{35}\text{N}_6\text{O}_4\text{S}$ ($\text{M} + \text{H}$) $^+$, 563.2440; found, 563.2441.

3,4,5-trimethoxy-N-(1-(5-methyl-2-((3-phenylpropyl)thio)-[1,2,4]triazolo [1,5-a]pyrimidin-7-yl)piperidin-3-yl)benzamide (**5p**), white solid, yield: 77%. m.p.: 154–156 °C. ^1H NMR (400 MHz, DMSO- d_6) δ 8.37 (d, $J = 7.3$ Hz, 1H), 7.39–7.05 (m, 7H), 5.48 (s, 1H), 4.13 (d, $J = 6.4$ Hz, 1H), 3.81 (s, 6H), 3.70 (s, 3H), 3.34 (d, $J = 10.1$ Hz, 1H), 3.22 (d, $J = 12.4$ Hz, 1H), 3.10 (t, $J = 7.0$ Hz, 2H), 2.80 (dd, $J = 20.4, 9.8$ Hz, 2H), 2.70 (t, $J = 7.5$ Hz, 2H), 2.16 (s, 3H), 2.04–1.83 (m, 4H), 1.73–1.54 (m, 2H). ^{13}C NMR (100 MHz, DMSO- d_6) δ 165.91, 161.20, 159.88, 158.13, 157.38, 153.03, 141.74, 140.69, 129.79, 128.79, 128.77, 126.28, 105.54, 96.06, 60.57, 56.90, 56.54, 47.67, 44.83, 44.02, 34.53, 31.53, 30.46, 28.99, 23.68, 22.14. HRMS (ESI): m/z calcd for $\text{C}_{30}\text{H}_{37}\text{N}_6\text{O}_4\text{S}$ ($\text{M} + \text{H}$) $^+$, 577.2597; found, 577.2597.

3,4,5-trimethoxy-N-(1-(5-methyl-2-((naphthalen-1-yl)methyl)thio)-[1,2,4]triazolo [1,5-a]pyrimidin-7-yl)piperidin-3-yl)benzamide (**5q**), white solid, yield: 88%. m.p.: 174–176 °C. ^1H NMR (400 MHz, DMSO- d_6) δ 8.37 (d, $J = 7.4$ Hz, 1H), 8.18 (d, $J = 8.1$ Hz, 1H), 7.95 (d, $J = 7.8$ Hz, 1H), 7.86 (d, $J = 8.2$ Hz, 1H), 7.70–7.48 (m, 3H), 7.42 (t, $J = 7.6$ Hz, 1H), 7.17 (s, 2H), 5.51 (s, 1H), 4.89 (s, 2H), 4.12 (d, $J = 6.1$ Hz, 1H), 3.81 (s, 6H), 3.70 (s, 3H), 3.34 (d, $J = 9.7$ Hz, 1H), 3.20 (d, $J = 12.6$ Hz, 1H), 2.79 (t, $J = 11.1$ Hz, 2H), 2.19 (s, 3H), 1.90 (t, $J = 18.3$ Hz, 2H), 1.72–1.53 (m, 2H). ^{13}C NMR (100 MHz, DMSO- d_6) δ 165.93, 161.08, 160.29, 158.37, 157.47, 153.02, 140.67, 133.94, 131.52, 129.75, 129.10, 128.48, 127.86, 126.79, 126.38, 125.93, 124.35, 105.52, 96.13, 60.57, 56.53, 47.54, 44.74, 43.95, 32.89, 28.90, 23.86, 22.01. HRMS (ESI): m/z calcd for $\text{C}_{32}\text{H}_{35}\text{N}_6\text{O}_4\text{S}$ ($\text{M} + \text{H}$) $^+$, 599.2440; found, 599.2439.

N-(1-(2-(allylthio)-5-methyl-[1,2,4]triazolo [1,5-a]pyrimidin-7-yl)piperidin-3-yl)-3,4,5-trimethoxybenzamide (**5r**), white solid, yield: 82%. m.p.: 138–140 °C. ^1H NMR (400 MHz, DMSO- d_6) δ 8.37 (d, $J = 7.4$ Hz, 1H), 7.17 (s, 2H), 5.97 (m, 1H), 5.48 (s, 1H), 5.26 (d, $J = 17.0$ Hz, 1H), 5.06 (d, $J = 10.0$ Hz, 1H), 4.12 (d, $J = 6.6$ Hz, 1H), 3.82 (s, 6H), 3.78 (d, $J = 6.8$ Hz, 2H), 3.70 (s, 3H), 3.34 (d, $J = 9.5$ Hz, 1H), 3.22 (d, $J = 12.6$ Hz, 1H), 2.80 (dd, $J = 21.9, 10.7$ Hz, 2H), 2.16 (s, 3H), 1.96–1.85 (m, 2H), 1.71–1.56 (m, 2H). ^{13}C NMR (100 MHz, DMSO- d_6) δ 165.92, 160.69, 160.32, 158.40, 157.47, 153.02, 140.66, 134.87, 129.79, 117.87, 105.51, 95.98, 60.57, 56.53, 47.64, 44.81, 44.01, 33.62, 28.98, 23.88, 22.12. HRMS (ESI): m/z calcd for $\text{C}_{24}\text{H}_{31}\text{N}_6\text{O}_4\text{S}$

(M + H)⁺, 499.2127; found, 499.2126.

N-(1-(2-(((1H-benzo[d]imidazole-2-yl)methyl)thio)-5-methyl-[1,2,4]triazolo [1,5-a]pyrimidin-7-yl)piperidin-3-yl)-3,4,5-trimethoxybenzamide (**5s**), white solid, yield: 84%. m.p.: 174–177 °C. ¹H NMR (400 MHz, DMSO-*d*₆) δ 8.39 (d, *J* = 7.4 Hz, 1H), 7.52 (dd, *J* = 5.2, 3.3 Hz, 2H), 7.24–7.10 (m, 4H), 5.52 (s, 1H), 4.62 (s, 2H), 4.16 (d, *J* = 6.5 Hz, 1H), 3.82 (s, 6H), 3.70 (s, 3H), 3.40 (d, *J* = 9.3 Hz, 1H), 3.27 (d, *J* = 12.5 Hz, 1H), 2.85 (dd, *J* = 19.9, 9.6 Hz, 2H), 2.18 (s, 3H), 1.92 (dd, *J* = 18.5, 11.5 Hz, 2H), 1.81–1.54 (m, 2H). ¹³C NMR (100 MHz, DMSO-*d*₆) δ 165.97, 161.21, 160.49, 158.77, 157.67, 153.02, 151.92, 140.67, 129.79, 122.27, 105.53, 95.99, 60.58, 56.54, 47.54, 44.80, 43.92, 28.96, 28.52, 24.18, 22.04. HRMS (ESI): *m/z* calcd for C₂₉H₃₃N₈O₄S (M + H)⁺, 589.2345; found, 589.2344.

N-(1-(2-((4-chlorobenzyl)thio)-5-ethyl- [1,2,4]triazolo [1,5-a]pyrimidin-7-yl)piperidin-3-yl)-3,4,5-trimethoxybenzamide (**5t**), white solid, yield: 89%. m.p.: 162–166 °C. ¹H NMR (400 MHz, DMSO-*d*₆) δ 8.38 (d, *J* = 7.3 Hz, 1H), 7.45 (d, *J* = 7.8 Hz, 2H), 7.34 (d, *J* = 7.9 Hz, 2H), 7.17 (s, 2H), 5.50 (s, 1H), 4.38 (s, 2H), 4.13 (s, 1H), 3.82 (s, 6H), 3.70 (s, 3H), 3.35 (d, *J* = 11.6 Hz, 1H), 3.23 (d, *J* = 12.6 Hz, 1H), 2.81 (dd, *J* = 20.6, 10.0 Hz, 2H), 2.44 (m, 2H), 1.91 (t, *J* = 15.3 Hz, 2H), 1.74–1.54 (m, 2H), 1.16 (t, *J* = 7.5 Hz, 3H). ¹³C NMR (101 MHz, DMSO) δ 165.95, 165.18, 160.79, 158.33, 157.65, 153.03, 140.70, 138.23, 132.06, 131.07, 129.74, 128.74, 105.54, 94.84, 60.58, 56.54, 47.40, 44.63, 43.89, 34.02, 30.36, 28.81, 21.86, 13.77. HRMS (ESI): *m/z* calcd for C₂₉H₃₄ClN₆O₄S (M + H)⁺, 597.2051; found, 597.2050.

N-(1-(2-((4-chlorobenzyl)thio)-5-phenyl- [1,2,4]triazolo [1,5-a]pyrimidin-7-yl)piperidin-3-yl)-3,4,5-trimethoxybenzamide (**5u**), white solid, yield: 86%. m.p.: 170–172 °C. ¹H NMR (400 MHz, DMSO-*d*₆) δ 8.39 (d, *J* = 7.2 Hz, 1H), 7.99 (d, *J* = 7.4 Hz, 2H), 7.54–7.30 (m, 7H), 7.18 (s, 2H), 6.15 (s, 1H), 4.43 (s, 2H), 4.17 (d, *J* = 6.3 Hz, 1H), 3.82 (s, 6H), 3.70 (s, 3H), 3.26 (d, *J* = 12.4 Hz, 2H), 2.84 (m, 2H), 1.92 (t, *J* = 12.2 Hz, 2H), 1.78–1.55 (m, 2H). ¹³C NMR (100 MHz, DMSO-*d*₆) δ 166.01, 161.29, 159.27, 158.81, 158.05, 153.04, 140.75, 139.46, 138.28, 132.07, 131.11, 129.66, 129.38, 128.77, 127.18, 105.56, 93.15, 60.59, 56.56, 46.97, 44.32, 43.67, 34.02, 28.55, 21.45. HRMS (ESI): *m/z* calcd for C₃₃H₃₄ClN₆O₄S (M + H)⁺, 645.2051; found, 645.2050.

N-(1-(2-((4-chlorobenzyl)thio)-5-methyl-6-pentyl- [1,2,4]triazolo [1,5-a]pyrimidin-7-yl)piperidin-3-yl)-3,4,5-trimethoxybenzamide (**5v**), white solid, yield: 85%. m.p.: 167–169 °C. ¹H NMR (400 MHz, DMSO-*d*₆) δ 8.33 (d, *J* = 7.4 Hz, 1H), 7.45 (d, *J* = 7.8 Hz, 2H), 7.34 (d, *J* = 7.8 Hz, 2H), 7.17 (s, 2H), 4.38 (s, 2H), 4.08 (s, 1H), 3.81 (s, 6H), 3.70 (s, 3H), 3.30 (d, *J* = 10.3 Hz, 1H), 3.17 (d, *J* = 12.4 Hz, 1H), 2.75 (dd, *J* = 20.4, 9.8 Hz, 2H), 2.46–2.36 (m, 2H), 2.24 (s, 3H), 1.88 (dd, *J* = 27.9, 12.3 Hz, 2H), 1.62 (m, 2H), 1.44–1.22 (m, 6H), 0.86 (t, *J* = 6.3 Hz, 3H). ¹³C NMR (100 MHz, DMSO-*d*₆) δ 165.86, 160.88, 157.11, 155.54, 153.01, 140.63, 138.22, 132.07, 131.08, 129.84, 128.73, 107.48, 105.50, 60.56, 56.52, 48.10, 45.11, 44.25, 34.06, 31.82, 29.23, 29.11, 25.96, 22.59, 21.28, 14.45. HRMS (ESI): *m/z* calcd for C₃₃H₄₂ClN₆O₄S (M + H)⁺, 653.2677; found, 653.2676.

4.4. Cell culture

Human prostatic carcinoma cell line PC3, human breast adenocarcinoma cell line MCF-7, human gastric carcinoma cell line MGC-803, human lung carcinoma cell line PC9, normal human prostatic cell line WPMY-1 were all purchased from the Cell Bank of Shanghai Institute of Biochemistry and Cell Biology. They were cultured in RPMI-1640 and DMEM complete medium (Solarbio, China) at 37 °C in a 5% CO₂ humidified atmosphere.

4.5. MTT assay

Briefly, cells were incubated with serial concentrations of the compounds for 24 h, 48 h and 72 h, respectively. 20 μl MTT solution

was added to each well and then the plates were incubated for another 4 h. Finally, absorbance values were measured by an enzyme-linked immunosorbent assay reader (BioTek, USA) at 490 nm. The cell viability and IC₅₀ were calculated by SPSS20 software.

4.6. Colony formation assay

Cells were seeded into 6-well plates at a concentration of 800 cells per well. Then they were respectively incubated with 0.125 μM, 0.25 μM and 0.5 μM compound **5q** for 6 days. After that, cells were stained by 0.1% crystal violet solution at room temperature for 30 min and then photographed. Subsequently, the crystal violet crystals were dissolved in 75% ethanol and the absorbance values were measured by an enzyme-linked immunosorbent assay reader at 595 nm.

4.7. Cell cycle assay

PC3 cells seeded in 6-well plates at a concentration of 4 × 10⁵ cells per well were respectively incubated with 1 μM, 2 μM and 4 μM compound **5q** for 24 h. Subsequently, cells were harvested and stained in 500 μl Propidium Iodide solution (PI 1 mg/ml, RNase A 10 mg/ml, Solarbio) at room temperature away from light for 30 min. Staining cells were detected and analyzed by flow cytometry (BD Bioscience, USA).

4.8. Hoechst 33342 staining

Cells were incubated with indicated concentrations of compound **5q** in 12-well plate for 48 h. Then cells were stained by Hoechst 33342 buffer (10 μg/ml, Solarbio) for 20 min in the dark. The morphological changes and nuclear fragmentation were imaged by an inverted fluorescence microscope (Nikon Eclipse TE 2000-S).

4.9. ROS assay

Cells seeded in 6-well plates were incubated with indicated concentrations of compound **5q** for 24 h. Then cells were washed in PBS and stained by 10 μM dichlorodihydrofluorescein diacetate (DCFH-DA, Beyotime) at 37 °C for 20 min in the dark. Then cells were collected and detected by flow cytometry.

4.10. Cell apoptosis assay

Cells plated in 6-well plates were respectively incubated with 1 μM, 2 μM and 4 μM compound **5q** for 48 h. Then cells were collected and stained by 200 μl binding buffer including 2 μl Annexin V-FITC and 2 μl PI (Beyotime) for 10 min at room temperature in the dark. Lastly, flow cytometry was used to detect the apoptotic cells.

4.11. Migration assay

For the wound healing assay, when PC3 cells seeded in 6-well plates reached to the density of 90%, they were scraped off using a sterile yellow pipette tip and photographed. Subsequently, cells were incubated with 0.25 μM, 0.5 μM and 1 μM compound **5q** for 48 h, and then each well was photographed again.

For the transwell assay, 600 μl fresh medium with 20% FBS were added to the substrate of the 24-well plates. 2 × 10⁴ cells per well were seeded and incubated with indicated concentrations of compound **5q** in the upper chambers for 48 h. Then these chambers were stained by 0.1% crystal violet solution and photographed.

4.12. Western blotting analysis

Cells incubated with indicated concentrations of compound 5q for 24 h or 48 h were collected with trypsin and total proteins were extracted in lysis buffer. BCA protein assay kit (Solarbio) was used to determine the concentration of the total proteins. Then these samples were detected by standard protocol of Western blot as described before.

Declaration of competing interest

The authors declare that they have no known competing financial interests or personal relationships that could have appeared to influence the work reported in this paper.

Acknowledgment

This work was supported by the financial support from the National Natural Science Foundation of China (Nos. 81773562, 81973177 and 81703326).

Appendix A. Supplementary data

Supplementary data to this article can be found online at <https://doi.org/10.1016/j.ejmech.2020.112471>.

References

- [1] T.T. Ashburn, K.B. Thor, Drug repositioning: identifying and developing new uses for existing drugs, *Nat. Rev. Drug Discov.* 3 (2004) 673–683.
- [2] F. Pammolli, L. Magazzini, M. Riccaboni, The productivity crisis in pharmaceutical R&D, *Nat. Rev. Drug Discov.* 10 (2011) 428–438.
- [3] H.A.M. Mucke, E. Mucke, Sources and targets for drug repurposing: landscape transitions in therapeutic space, *Assay Drug Dev. Technol.* 13 (2015) 319–324.
- [4] N. Nosengo, New tricks for old drugs, *Nature* 534 (2016) 314–316.
- [5] W.A. Chow, C. Jiang, M. Guan, Anti-HIV drugs for cancer therapeutics: back to the future? *Lancet Oncol.* 10 (2009) 61–71.
- [6] S. Pushpakom, F. Iorio, P.A. Eyers, K.J. Escott, S. Hopper, A. Wells, A. Doig, T. Williams, J. Latimer, C. McNamee, A. Norris, P. Sanseau, D. Cavalla, M. Pirmohamed, Drug repurposing: progress, challenges and recommendations, *Nat. Rev. Drug Discov.* 18 (2019) 41–58.
- [7] Y. Cha, T. Erez, I.J. Reynolds, D. Kumar, J. Ross, G. Koytger, R. Kusko, B. Zeskind, S. Risso, E. Kagan, S. Papapetropoulos, I. Grossman, D. Laifenfeld, Drug repurposing from the perspective of pharmaceutical companies, *Br. J. Pharmacol.* 175 (2018) 168–180.
- [8] J.-P. Jourdan, R. Bureau, C. Rochais, P. Dallemagne, Drug repositioning: a brief overview, *J. Pharm. Pharmacol.* (2020), <https://doi.org/10.1111/jphp.13273>.
- [9] Hatzimouratidis Konstantinos, Sildenafil I in the treatment of erectile dysfunction: an overview of the clinical evidence, *Clin. Interv. Aging* 4 (2006) 403–414.
- [10] S.E.S. Inghal, J.A.M. Ehta, R.A.D. Esikan, D.A.A. Yers, P.A.R. Oberson, P.A.E. Ddlemon, N.I.M. Unshi, E.L.A. Naissie, C.A.W. Ilson, M.A.D. Hodapkar, J.E.Z. Eldis, B.A.B. Arlogie, Antitumor activity OF thalidomide IN refractory multiple myeloma, *N. Engl. J. Med.* 341 (1999) 1565–1571.
- [11] L. Urquhart, Market watch: top drugs and companies by sales in 2017, *Nat. Rev. Drug Discov.* 17 (2018) 232.
- [12] K.E. Ng, B.C.P.S. PharmD, Xofluza (baloxavir marboxil) for the treatment of acute uncomplicated influenza, *Pharmacol. Therapeut.* 44 (2019) 9–11.
- [13] S. Zhu, X. Guo, K. Geary, D. Zhang, Emerging therapeutic strategies for COVID-19 patients, *Discoveries* 8 (2020) e105–e110.
- [14] A.Y. Pawar, Combating devastating COVID-19 by drug repurposing, *Int. J. Antimicrob. Agents* (2020) 105984–105986.
- [15] J.-M. Rolain, P. Colson, D. Raoult, Recycling of chloroquine and its hydroxyl analogue to face bacterial, fungal and viral infections in the 21st century, *Int. J. Antimicrob. Agents* 30 (2007) 297–308.
- [16] P. Colson, J.-M. Rolain, D. Raoult, Chloroquine for the 2019 novel coronavirus SARS-CoV-2, *Int. J. Antimicrob. Agents* 55 (2020) 105923.
- [17] M. Wang, R. Cao, L. Zhang, X. Yang, J. Liu, M. Xu, Z. Shi, Z. Hu, W. Zhong, G. Xiao, Remdesivir and chloroquine effectively inhibit the recently emerged novel coronavirus (2019-nCoV) in vitro, *Cell Res.* 30 (2020) 269–271.
- [18] X. Xu, M. Han, T. Li, W. Sun, D. Wang, B. Fu, Y. Zhou, X. Zheng, Y. Yang, X. Li, X. Zhang, A. Pan, H. Wei, Effective Treatment of Severe COVID-19 Patients with Tocilizumab, *ChinaXiv*, 2020, <https://doi.org/10.12074/202003.00026>.
- [19] D. Bhupesh, S. Navajit, Bioequivalence study of troxipide tablet formulations, *J. Bioequivalence Bioavailab.* (2010) 50–54, 02.
- [20] S. Wang, L.-J. Zhao, Y.-C. Zheng, D.-D. Shen, E.-F. Miao, X.-P. Qiao, L.-J. Zhao, Y. Liu, R. Huang, B. Yu, H.-M. Liu, Design, synthesis and biological evaluation of [1,2,4]triazolo[1,5-a]pyrimidines as potent lysine specific demethylase 1 (LSD1/KDM1A) inhibitors, *Eur. J. Med. Chem.* 125 (2017) 940–951.
- [21] S. Wang, L. Zhao, X.-J. Shi, L. Ding, L. Yang, Z.-Z. Wang, D. Shen, K. Tang, X.-J. Li, M. Mamun, H. Li, B. Yu, Y.-C. Zheng, S. Wang, H.-M. Liu, Development of highly potent, selective, and cellular active triazolo[1,5-a]pyrimidine-based inhibitors targeting the DCN1-UBC12 protein-protein interaction, *J. Med. Chem.* 62 (2019) 2772–2797.
- [22] S. Wang, D. Shen, L. Zhao, X. Yuan, J. Cheng, B. Yu, Y. Zheng, H. Liu, Discovery of [1,2,4]triazolo[1,5-a]pyrimidine derivatives as new bromodomain-containing protein 4 (BRD4) inhibitors, *Chin. Chem. Lett.* 31 (2020) 418–422.
- [23] S. Wang, Z.-R. Li, F.-Z. Suo, X.-H. Yuan, B. Yu, H.-M. Liu, Synthesis, structure-activity relationship studies and biological characterization of new [1,2,4]triazolo[1,5-a]pyrimidine-based LSD1/KDM1A inhibitors, *Eur. J. Med. Chem.* 167 (2019) 388–401.
- [24] Z.-R. Li, S. Wang, L. Yang, X.-H. Yuan, F.-Z. Suo, B. Yu, H.-M. Liu, Experience-based discovery (EBD) of aryl hydrazines as new scaffolds for the development of LSD1/KDM1A inhibitors, *Eur. J. Med. Chem.* 166 (2019) 432–444.
- [25] N. Zhao, K.-t. Tian, K.-g. Cheng, T. Han, Xu Hu, D.-h. Li, Z.-l. Li, H.-m. Hua, Antiproliferative activity and apoptosis inducing effects of nitric oxide donating derivatives of evodiamine, *Bioorg. Med. Chem.* 24 (2016) 2971–2978.
- [26] D. Hanahan, R.A. Weinberg, Hallmarks of cancer: the next generation, *Cell* 144 (2011) 646–674.
- [27] J. Li, X.K. Yang, X.X. Yu, M.L. Ge, W.L. Wang, J. Zhang, Y.D. Hou, Overexpression of p27KIP1 induced cell cycle arrest in G1 phase and subsequent apoptosis in HCC-9204 cell line, *World J. Gastroenterol.* 6 (2000) 513–521.
- [28] K. Sinha, J. Das, P.B. Pal, P.C. Sil, Oxidative stress: the mitochondria-dependent and mitochondria-independent pathways of apoptosis, *Arch. Toxicol.* 87 (2013) 1157–1180.
- [29] C.-F. Lee, J.-S. Yang, F.-J. Tsai, N.-N. Chiang, C.-C. Lu, Y.-S. Huang, C. Chen, F.-A. Chen, Kaempferol induces ATM/p53-mediated death receptor and mitochondrial apoptosis in human umbilical vein endothelial cells, *Int. J. Oncol.* 48 (2016) 2007–2014.
- [30] P. Li, D. Nijhawan, I. Budihardjo, S.M. Srinivasula, M. Ahmad, E.S. Alnemri, X. Wang, Cytochrome c and dATP-dependent formation of apaf-1/caspase-9 complex initiates an apoptotic protease cascade, *Cell* 97 (1997) 479–489.
- [31] R.-Z. Huang, G.-B. Liang, X.-C. Huang, B. Zhang, M.-M. Zhou, Z.-X. Liao, H.-S. Wang, Discovery of dehydroabietic acid sulfonamide based derivatives as selective matrix metalloproteinases inactivators that inhibit cell migration and proliferation, *Eur. J. Med. Chem.* 138 (2017) 979–992.
- [32] L. Tahtamouni, M. Ahram, J. Koblinski, C. Rolfo, Molecular regulation of cancer cell migration, invasion, and metastasis, *Anal. Cell Pathol.* 2019 (2019), 1356508.